Dating Water and Ice Using the Radioactivity of Atmospheric ^{85}Kr

Rahul Mazumder(bmat2019), Md Rahil Miraj(bmat2013),
Mainak Samanta(bmat2012), Ankan Kar(bmat2001)*
B.Math(Second Year)
Indian Statistical Institute
Bengaluru, Karnataka, India

(Dated: December 24, 2021)

Abstract

With a half-life of 10.7 years, the noble gas radio-isotope ^{85}Kr is perfectly suited as a tracer for dating water and ice that is formed during the first half-century.

Using data from the monitoring stations in the southern hemisphere, a 7-degree polynomial is derived to model the data. Fitting a linear curve to the data shows that the atmospheric ^{85}Kr concentration increased linearly between 1980 and 2005 and concentrations stabilised thereafter. The data collected from the northern hemispheric monitoring stations have been used to calculate an interhemispheric exchange time of 1.25 years.

*Electronic address: rahulmazumder002@gmail.com, rahilmiraj@gmail.com, mainaksmnt@gmail.com, ankankar2002@gmail.com

Contents

I. INTRODUCTION

For dating water and ice, ^{85}Kr is considered as the perfect tracer during the past 50 years. This is made possible by its appropiate half-life of 10.739 ± 0.014 years [2]. Being a noble gas it is chemically inert and do not involve in any geochemical processes. Hence, the ratio of ^{85}Kr and the stable krypton remains unchanhged while transporting from the atmosphere into hydrological systems, and the only process that alters the ^{85}Kr concentrations within these systems are the radioactive decay and mixing.

1.1 Why use Krypton ?

The question may arise that why ^{85}Kr is preferred as a tracer. This is because the different other tracers which are used have several drawbacks which ^{85}Kr doesn't have like ambiguous tracer ages of concentrations due to its peak shaped input function, decreasing atmospheric activity concentration and significantly lower concentrations in precipitations in southern compared to northern hemisphere of Tritium, sensitivity to air due to low solubility and underground generation of SF_6, and declining input functions resulting in decreased sensitivity on short timescales in addition to toxicity under anoxic conditions of CFCs. Being devoid of these limitations [3][4], ^{85}Kr is the most robust tracer for dating hydrological systems on 5-40 years timescales, especially in the southern hemisphere.

1.2 Collection of Krypton

Since about a half century, ^{85}Kr analysis was taken place by detecting the decay counting in low background gas proportional counters [5]. We have a modern atmospheric $^{85}Kr/Kr$ isotope ratio approximately 2×10^{-11} [11], so to limit the routine application to groundwater studies[8] we require a large water sample volumes in the order of hundreds of liters for the analysis. To get rid of this requirement of huge samples, a laser-based atom counting method, Atom Trap Trace Analysis (ATTA)[6] is used. This method reduces the sample size requirements and measurement time drastically to a few liters of water and a throughput of up to 6 samples per day [7]. It seems, this will make ^{85}Kr dating of ocean water and ice more feasible and will increase the demand for ^{85}Kr dating in the upcoming times.

1.3 Sources of Krypton

It has been found that krypton is less abundant with an atmospheric concentration of 1.099 ± 0.009 *ppmv*, than the lighter noble gases [9]. But, since cosmic ray induced neutron capture according to the $^{85}Kr(n,\gamma)^{85}Kr$ reaction produces ^{85}Kr in the upper atmosphere, we get the anthropogenic contributions to the global atmospheric ^{85}Kr budget about 4 orders of magnitude higher [12]. Our largest sources for ^{85}Kr are the nuclear reprocessing plants and all other ^{85}Kr emitters together contribute less than 1% of global inventory [13]. ^{85}Kr is accumulated in the fuel rods of nuclear power reactors as a fission product of ^{235}U and ^{239}Pu. When the rods are de-cladded and subsequently dissolved in the nitric acid, these ^{85}Kr are released, during reprocessing. [14]

Since there is a direct link between Pu production and ^{85}Kr emissions, the isotope is very important for the verification of the nuclear arms control treaties. All relevant ^{85}Kr sources are located in the northern hemisphere as the first significant anthropogenic ^{85}Kr emissions into the atmosphere was taken place in the context of Pu production for the US nuclear weapons program between 1943 and 1945, [15]. Nowadays, ^{85}Kr is predominantly emitted from the civil nuclear reprocessing facilities, but it was already used in the late 1940s and early 1950s to determine the weapons Pu production from the total atmospheric ^{85}Kr content [16]. Also, the amount of produced Pu can be calculated from the ^{85}Kr measurements near a reprocessing plant [17].

There are two significant effects of the global distribution of nuclear reprocessing plants:

1. The atmospheric ^{85}Kr activity concentrations in the northern hemisphere are on average about 10% higher than in the southern hemisphere.

2. Depending on the distance to the plant, the emission events in reprocessing plants result in significant variations in local ^{85}Kr activity concentrations, the emitted ^{85}Kr amount and the meteorological conditions [18].

The high and variable ^{85}Kr background caused by strong civil emitters like the reprocessing plants La Hague in the west of France and Sellafield in the south of Great Britain is a big challenge to use the tracer for verification of nuclear arms control treaties [20].

We need a good knowledge of the past atmospheric ^{85}Kr concentrations in the area where the water of the investigated system last equilibrated with the atmosphere to use ^{85}Kr as a dating tracer. So, these past concentrations are essential to track monitoring stations. With

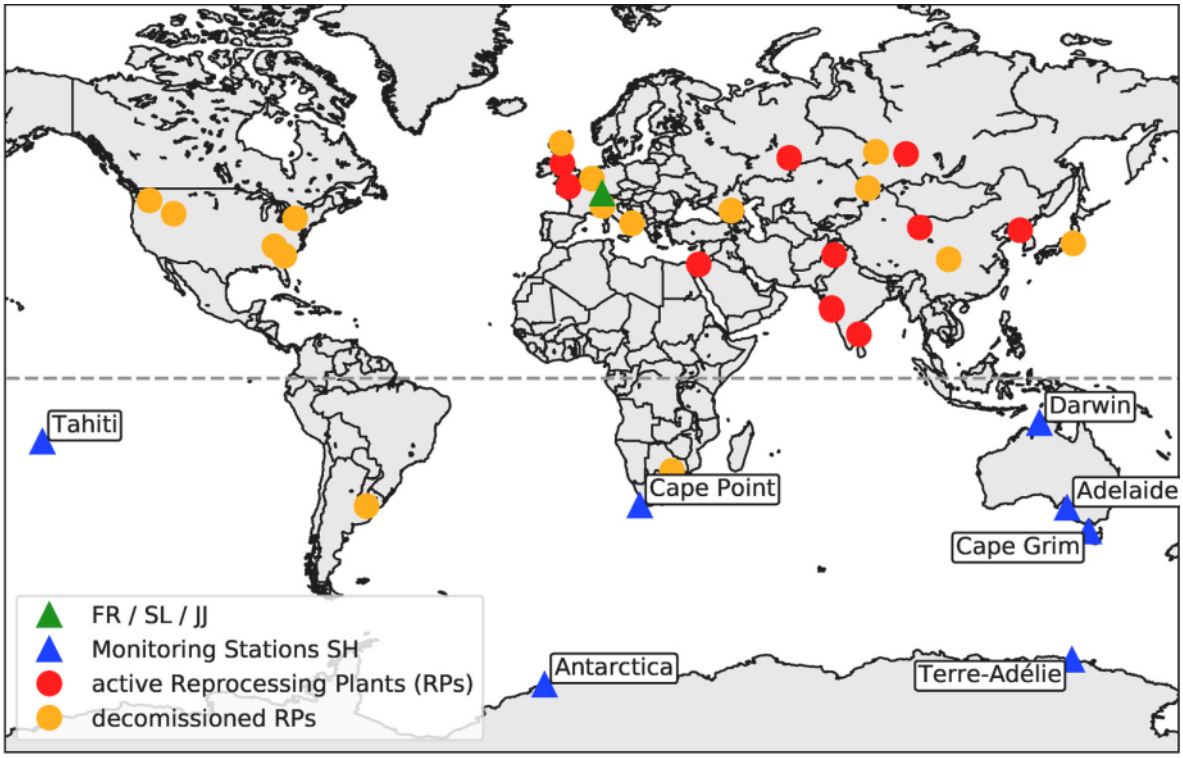

FIG. 1: The map shows all relevant active (red) and decommissioned (orange) reprocessing plants (RPs) based on [19] as well as all 7 krypton moni- toring stations in the southern hemisphere operated by various institutions, mostly in cooperation with the Bundesamt für Strahlenschutz (BfS) (blue). The green triangle symbolizes the monitoring stations Freiburg (FR), Schauinsland (SL) and Jungfraujoch (JJ)[1].

collaboration to about 20 research facilities around the globe, the largest ^{85}Kr data set is gathered by the Bundesamt für Strahlenschutz (BfS) in Germany to generate atmospheric ^{85}Kr series from about a half century [18].

1. Between March 1968 to October 1977, a systematic study of atmospheric ^{85}Kr concentrations in the southern hemisphere was performed by the Office of Atomic Energy in France. It is the earliest known study. They analysed about 20 air samples collected on Tahiti and about 30 air samples gathered during polar expeditions to Terre-Adélie [21][22].

2. In the year 1983, at Neumayer station in Antarctica, a continuous air sampling for ^{85}Kr analysis had started and about 400 atmospheric samples were taken till 2008, which was the longest record in the southern hemisphere.

3. Between 1985 and 1997, atmospheric air was sampled at Cape Point in South Africa

and at Cape Grim in Tasmania [23]. The same thing was done at Darwin in Australia from 2007 to 2010 [24].

4. Since 2015, the only operational monitoring station in the southern hemisphere is located at the Commonwealth Scientific and Industrial Research Organization (CSIRO) in Adelaide, South Australia.

All the mentioned monitoring stations and both active as well as decommissioned nuclear reprocessing plants are shown in Fig1.

1.4 Specifications Table

Subject : Atmospheric Science

Specific subject area : Monitoring of the atmospheric ^{85}Kr concentrations in ground level air in the northern and southern hemisphere

Type of data : Excel file in data repository: Table, Figure

How data were acquired : The ^{85}Kr activity concentration data were acquire after gaschromatographic separation of krypton followed by β-decay counting of ^{85}Kr in gas proportional counters.

Data format : Raw

Parameters for data collection : The krypton was sampled from ground level air and the monitoring stations were carefully chosen, to avoid contamination with locally produced ^{85}Kr.

Description of data collection : Primary data of the data collection comprises the Adelaide dataset and all samples of the Schauinsland, Jungfraujoch and Freiburg datasets taken since (December 2018). All other data is secondary data taken from the cited papers.

Data source location : Primary data sources:

Adelaide:

Institution: CSIRO

City/Town/Region: Adelaide

Country: South Australia

Lat/Lon of monitoring station: 34 ^{o}58' S 138 ^{o}38' E

Antarctica:

Institution: Institute of Environmental Physics, University Heidelberg, Germany

City/Town/Region: Georg von Neumayer Station

Country: Antarctica

Lat/Lon of monitoring station: 70 ^{o}40' S 08 ^{o}16' W

Cape Grim:

Institution: CSIRO and Institute of Environmental Physics, University Heidelberg, Germany

City/Town/Region: Tasmania

Country: Australia

Lat/Lon of monitoring station: 40 ^{o}41' S 144 ^{o}41' E

Cape Point:

Institution: Institute of Environmental Physics, University Heidelberg, Germany

City/Town/Region: Cape of Good Hope

Country: South Africa

Lat/Lon of monitoring station: 34 ^{o}32' S 18 ^{o}29' E

Darwin:

Institution: Supervising Scientist Division, Environment Australia

City/Town/Region: Darwin

Country: Australia

Lat/Lon of monitoring station: 12 ^{o}28' S 130 ^{o}50' E

Early Measurements:

Institutions: Physics Department, University Heidelberg, Germany

Institute of Environmental Physics, University Heidelberg, Germany Planck Institute for Nuclear Physics, Heidelberg, Germany

Max Planck Institute for Nuclear Physics, Freiburg-Schauinsland Branch, Germany

Institute for Atmospheric Radioactivity (IAR), Federal Office of Civil Defence, Freiburg, Germany

Commissariat a l'Energie Atomique, Department de la Protection Sanitaire, Fontenay-aux-Roses, France

Air Resources Laboratories, National Oceanic and Atmospheric Administration, Silver Spring, MD 20910, U.S.A

Freiburg:

Institution: Bundesamt für Strahlenschutz

City/Town/Region: Freiburg

Country: Germany

Lat/Lon of monitoring station: 48 ^{o}00' N 07 ^{o}51' E

Jungfraujoch:

Institution: Bundesamt für Strahlenschutz

City/Town/Region: Berner Alps

Country: Swiss

Lat/Lon of monitoring station: 46 ^{o}24' N 08 ^{o}42' E

Schauinsland:

Institution: Bundesamt für Strahlenschutz

City/Town/Region: Freiburg

Country: Germany

Lat/Lon of monitoring station: 47 ^{o}55' N 07 ^{o}54' E

Tahiti:

Institution: Office of Atomic Energy

City/Town/Region: Tahiti

Country: French Polynesia

Lat/Lon of monitoring station: 17 ^{o}37' S 149 ^{o}28' W

Terre-Adélie:

Institution: Office of Atomic Energy

City/Town/Region: Eastern Antarctica

Country: Antarctica

Lat/Lon of monitoring station: 66 ^{o}40' S 140 ^{o}00' E

Data accessibility : Kersting, Arne; Bollhöfer, Andreas; Schlosser, Clemens; Schmid, Sabine; Konrad, Martina; Barry, Karen; Suckow, Axel (2020), "Atmospheric krypton-85 activity concentrations", Mendeley Data, V1, doi: 10.17632/p32bmw6rgs.1 Direct URL to data: https://data.mendeley.com/datasets/p32bmw6rgs/1

Related research article : Kersting, C. Schlosser, A. Bollhöfer und A. Suckow, "Evaluating 5 decades of atmospheric ^{85}Kr measurements in the southern hemisphere to derive an input function for dating water and ice with implications for interhemispheric circulation

and the global ^{85}Kr emission inventory."JournalofEnvironmentalRadioactivity".In Press: https://doi.org/10.1016/j.jenvrad.2020.106451

1.5 Data Description

The data collection consists of 11 data sets of atmospheric ^{85}Kr activity concentrations with 4 data sets from monitoring stations in the northern hemisphere ("Early Measurements NH", "Freiburg", "Schauinsland" and "Jungfraujoch") and 7 datasets from monitoring stations in the southern hemisphere ("Adelaide", "Antarctica", "Cape Grim", "Cape Point", "Darwin", "Tahiti" and "Terre-Adelie").

All measurements were conducted via β-decay counting in gas proportional counters with a measurement uncertainty of about 3%. However, for the data sets "Tahiti" and "Terre-Adelie" no errors were given in the original publications and a conservative estimate of 10% measurement uncertainty was taken.

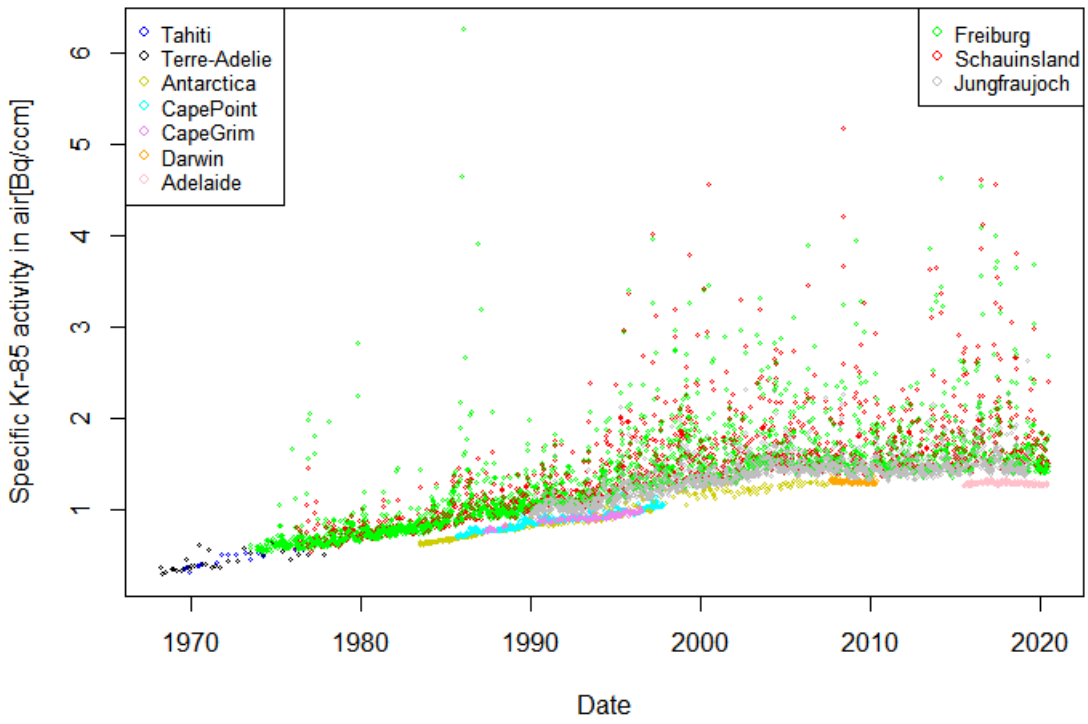

FIG. 2: Scatter plots for both Southern and Northern hemispheric data.

As seen in Fig.2 , the northern hemispheric data represents a coherent 60 years long series of measurements, while the southern hemispheric data set contains gaps of about 5

years between around 1980 and in the early 2010s. The ^{85}Kr activity concentrations in the Freiburg, Schauins- land and Jungfraujoch data set reach up to 6 Bq/m^3 air, while the southern hemispheric data do not exceed 1.5 Bq/m^3 air.

II. METHODS: CRYOGENIC PURIFICATION

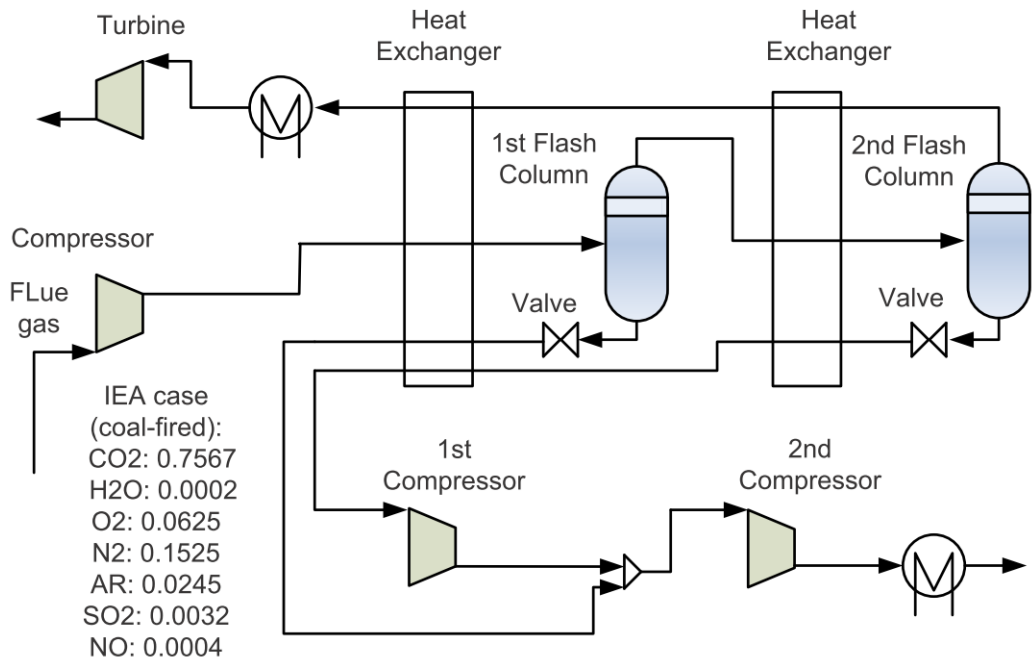

FIG. 3: A system sketch of Cryogenic Purification [33]

Over past five years the following sampling and measurement procedures are carried out in Adelaide's monitoring station. The procedure was same substantially in the past 50 years, so is applied for all the presented data.

For one week, about 10 m^3 of air is continuously pumped through a liquid nitrogen-cooled activated charcoal column at a pressure of 50 kPa to avoid condensation of O_2 and N_2 in the adsorbent. Water and CO_2 are frozen out before they reach the charcoal adsorbent while most of the krypton and xenon adsorb on the charcoal [10]. The column is removed from the liquid nitrogen after one week and to ensure continuous sampling, it is replaced immediately by a second column. At first, the first column is warmed up to the room temperature to desorb N_2 and O_2. Then it is heated to 300^{o}C to desorb the remaining gases from the charcoal, which are compressed at 500 kPa into a 1L aluminium bottle by

flushing the column with Helium (or Nitrogen).Then, for further cryogenic purification and subsequent analysis the pressurized bottles are sent to the laboratories of Bundesamt für Strahlenschutz in Freiburg, Germany.

In the second step of cryogenic purification, CO_2 is removed with 2M NaOH and subsequently using a silica gel column, water is also removed. To further remove air and trap the noble gases, the sample is then flushed through a small liquid nitrogen cooled activated charcoal column. The adsorbed and further concentrated noble gases subsequently are desorbed at 300^{o}C. Helium is used as a carrier gas in both the steps.

Then the krypton is separated from xenon using a 2-stage preparative gas chromatograph with methane as the carrier and counting gas. To measure the beta activity of ^{85}Kr [25], a typical sample yields between 2 and 5 mL of pure krypton, which is then injected into one of seven gas proportional counters. After the measurement, the volume of krypton in the proportional counter is determined quantitatively using a second gas chromatograph by comparison with a calibration gas of similar composition.

Including drifts and calibration uncertainties, the overall measurement uncertainty for an atmospheric ^{85}Kr measurement is about 3%. The detection limit for ^{85}Kr measurement is typically around $4mBq/m^3$ air.

III. POLYNOMIAL FITTING:

In this section, we will fit a Polynomial Regression model to describe the data. We will see that when we are increasing the degree of the fitted polynomial from 1 to 7, there is significant changes in the goodness of the fitting but the higher polynomial degrees do not change the goodness of the fit significantly. So, we will chose 7-degree polynomial as the best fitted curve to represent the data.

The polynomial regression model

$$y_i = \beta_0 + \beta_1 x_i + \beta_2 x_i^2 + \cdots + \beta_m x_i^m + \varepsilon_i \ (i = 1, 2, \ldots, n) \tag{1}$$

is expressed in a matrix form in terms of a design matrix $\mathbf{X}$, a response vector $\vec{y}$, a parameter vector $\vec{\beta}$, and a vector $\vec{\varepsilon}$ of random errors. The i-th row of $\mathbf{X}$ and $\vec{y}$ will contain the x and y values for the i-th sample data. Then the model can be written as a system of linear

equations:

$$\begin{bmatrix} y_1 \\ y_2 \\ y_3 \\ \vdots \\ y_n \end{bmatrix} = \begin{bmatrix} 1 & x_1 & x_1^2 & \dots & x_1^m \\ 1 & x_2 & x_2^2 & \dots & x_2^m \\ 1 & x_3 & x_3^2 & \dots & x_3^m \\ \vdots & \vdots & \vdots & \ddots & \vdots \\ 1 & x_n & x_n^2 & \dots & x_n^m \end{bmatrix} \begin{bmatrix} \beta_0 \\ \beta_1 \\ \beta_2 \\ \vdots \\ \beta_m \end{bmatrix} + \begin{bmatrix} \varepsilon_1 \\ \varepsilon_2 \\ \varepsilon_3 \\ \vdots \\ \varepsilon_n \end{bmatrix}, \tag{2}$$

which can be written as

$$\vec{y} = \mathbf{X}\vec{\beta} + \vec{\varepsilon}. \tag{3}$$

The vector of the estimated polynomial regression coefficients (using ordinary least squares estimation) is

$$\widehat{\vec{\beta}} = (\mathbf{X}^\mathsf{T}\mathbf{X})^{-1}\,\mathbf{X}^\mathsf{T}\vec{y} \tag{4}$$

assuming $m < n$ which is required for the matrix to be invertible. Then since $\mathbf{X}$ is a *Vandermonde* matrix, the invertibility condition is guaranteed to hold if all the x_i values are distinct. So, this is the unique least-squares solution.

In Table I, we are showing the R-squared values and Residual standard errors of the fitted polynomials for the data set of the Southern hemisphere.

Degree of fitted polynomial	R-squared	Deg. of freedom	Residual standard error
1	0.9058	1418	0.07476
2	0.9409	1417	0.05924
3	0.9758	1416	0.0379
4	0.9761	1415	0.03769
5	0.9777	1413	0.03643
6	0.9778	1412	0.03634
7	0.9782	1411	0.03606
8	0.9796	1410	0.03488
9	0.9806	1409	0.03406

TABLE I: Table for fitting of Southern hemisphere data set .

In Table II, we are showing the R-squared values and Residual standard errors of the fitted polynomials for the data set of the Northern hemisphere.

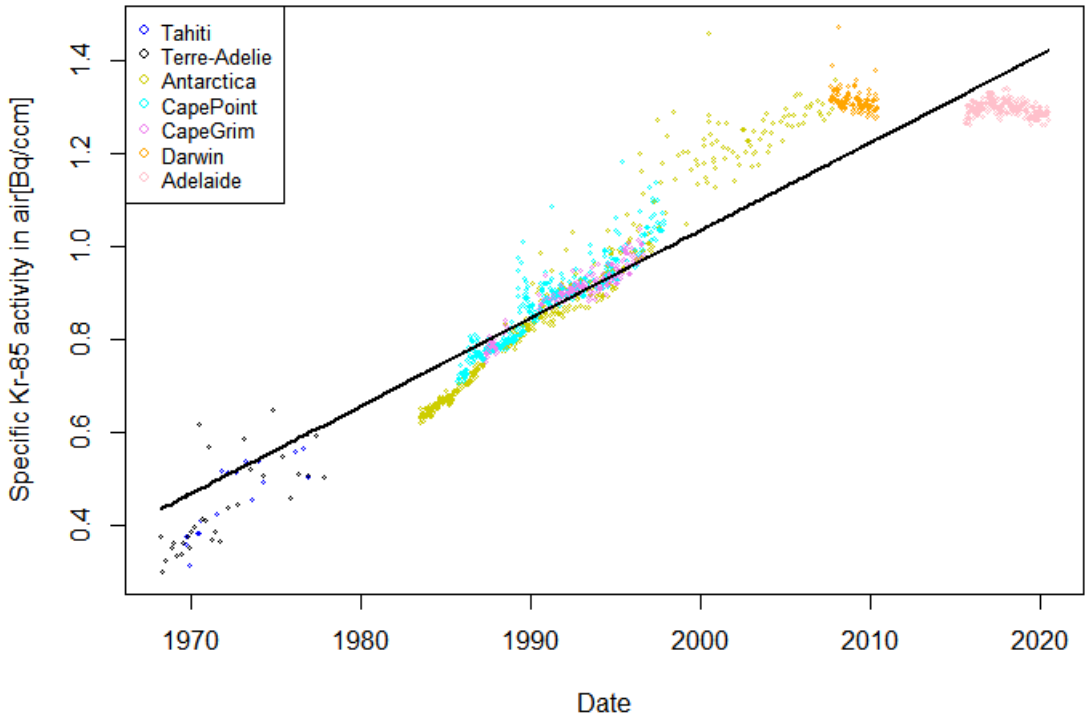

FIG. 4: Fitted linear model for Southern hemispheric data.

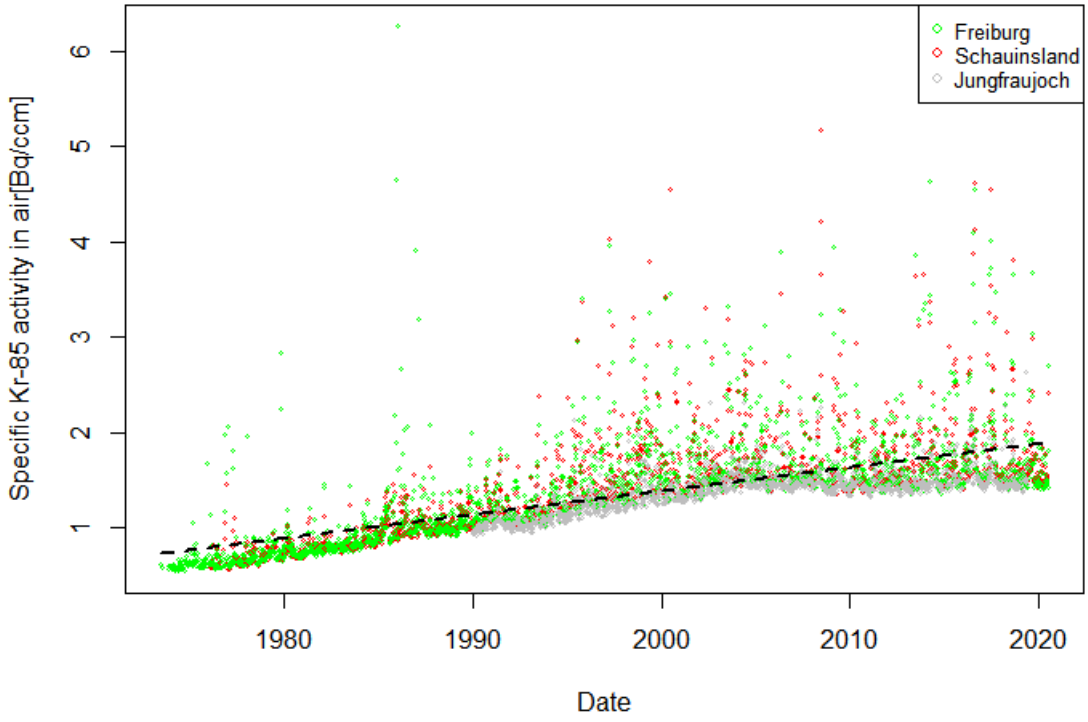

FIG. 5: Fitted linear model for Northern hemispheric data.

Degree of fitted polynomial	R-squared	Deg. of freedom	Residual standard error
1	0.4416	6138	0.346
2	0.4816	6137	0.3334
3	0.485	6136	0.3323
4	0.4881	6135	0.3314
5	0.4887	6134	0.3312
6	0.4907	6133	0.3306
7	0.4968	6132	0.3286
8	0.4972	6131	0.3285
9	0.4998	6130	0.3277

TABLE II: Table for fitting of Northern hemisphere data set .

Here, R^2 (R-squared) represents the proportion of variance of a dependent variable that is explained by an independent variable (or variables) in the model. In other words, it gives the percentage of observed variation that can be explained by the inputs of the model. Residual standard error is given by

$$\sqrt{\frac{\sum(y-\hat{y})}{df}}; \tag{5}$$

where,

y= the observed value

$\hat{y}$ = the predicted value

df = degree of freedom which is calculated by total number of observations - total number of parameters.

It is used to measure how well a regression model fits a database. The smaller the residual standard error, the better the regression model fits a database. So the R-squared is closer to 1 and the model is better fitted.

So, the fitted 7-degree polynomial for the Southern hemisphere data, shown in Fig 6 is:

$$0.98166+8.72954x-1.71778x^2-1.71441x^3-0.15422x^4+0.36638x^5+0.09899x^6+0.17500x^7 \tag{6}$$

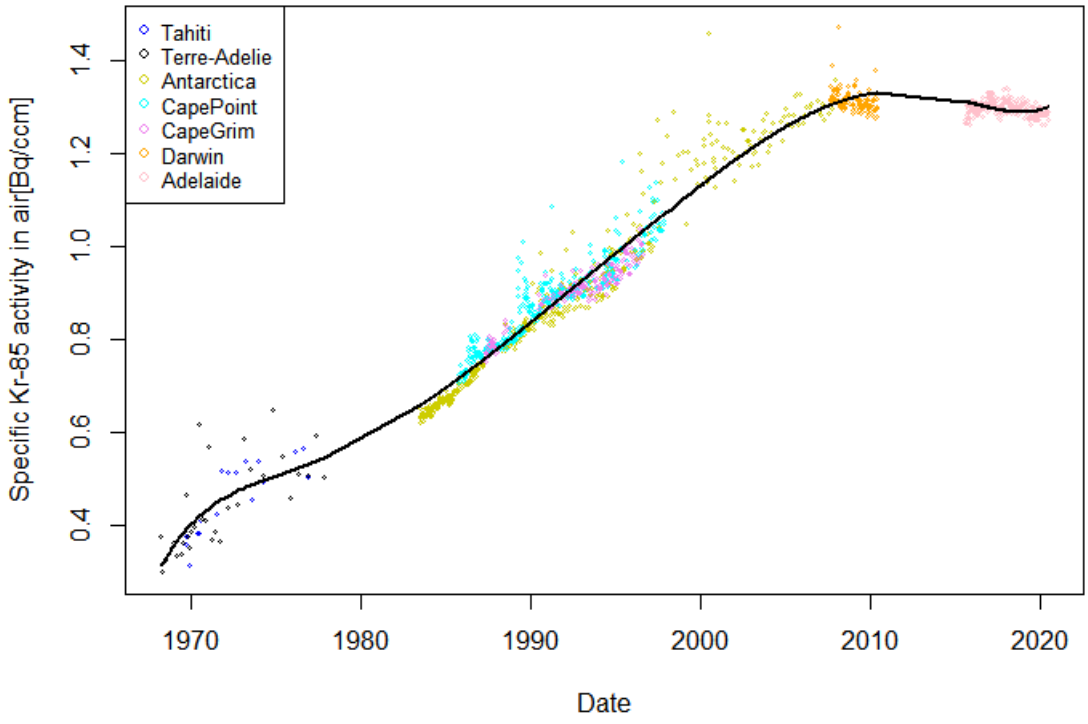

FIG. 6: Fitted 7-degree curve for Southern hemispheric data.

And, the fitted 7-degree polynomial for the Northern hemisphere data, shown in Fig 7 is:

$$1.373 + 24.105x - 7.254x^2 - 2.139x^3 + 2.004x^4 + 0.920x^5 - 1.627x^6 - 2.832x^7 \qquad (7)$$

IV. RESULTS AND DISCUSSIONS

The analysis of the entire data collection [26] is performed with R and can be reproduced following the description published in the corresponding MethodsX paper [26]. There are 255 ^{85}Kr measurements from 13th July,2015 to 17th June,2020 in the Adelaide dataset. There were weekly samplings and the data set is a complete record of ^{85}Kr activity concentrations in ground level air in Adelaide of the last 5 years,except for 2 weeks. The uncertainty of each measurement is about 3%.

3.1. Southern hemispheric input function

Fig.2 shows the atmospheric ^{85}Kr activity concentrations of all southern hemispheric monitoring stations plotted against sampling date.

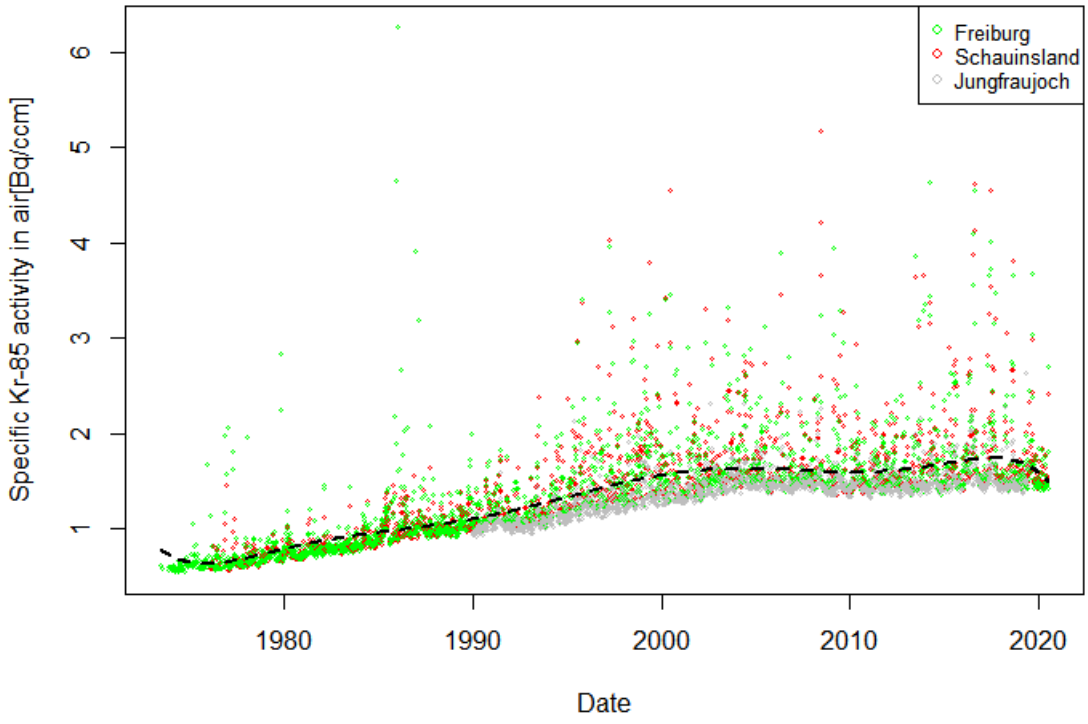

FIG. 7: Fitted 7-degree curve for Northern hemispheric data.

A linear regression in Fig.4 shows, that on average the ^{85}Kr concentration is decreased by just 3 mBq/(m^3 air year) as the sampling were initiated in July 2015. The fit to all southern hemispheric ^{85}Kr data is the best description of the input function for ^{85}Kr dating of water and ice that formed since 1968.

Still, there is a slight bias in the southern hemispheric data as the monitoring stations are at different degrees' latitude (Fig. 1). Darwin is the closest to the Intertropical Convergence Zone of all monitoring stations, so the chance of elevated atmospheric ^{85}Kr concentrations increases due to stronger influence from the northern hemisphere [24].

3.2. Seasonality of the Adelaide dataset

The Adelaide data set covers 5 Australian summers with the hottest months in December, January and February. Between July 2016 and July 2018, a seasonality is indicated by the data with peak concentrations in the summers of 2016-17 and 2017-18. But in the summer of 2015-16 as well as 2018-19 and 2019-20, there were zero significantly elevated ^{85}Kr concentrations. The effect might be due to the seasonality of the Hadley cell circulation over

Australia as has been shown in ^{7}Be data [27]. When the Intertropical Convergence Zone (ITCZ) is farthest to the south (during the Australian summer), northern hemispheric air with higher ^{85}Kr concentrations leaks into the southern hemisphere [28]. The location and strength of this event associated with the El-$Niño$ Southern Oscillation leads to the inter-hemispheric mixing at the ITCZ. During El-$Niño$ years affecting the Australian summer in 2015-16 and 2018-19, the convective upwelling at the ITCZ was located in the Pacific center and thus, did not significantly influence Adelaide. During La $Niña$ years however, a strong convective pattern is located right in the north of Australia triggering a potential northern hemispheric ^{85}Kr flux towards the South of Australia. To strengthen this hypothesis, further sampling along a north-south transect during strong La $Niña$ years is required. Interestingly, in Darwin, an area strongly influenced by the annual movement of the ITCZ, no seasonality was evident in the data [24] although the Australian summer 2007/08 and 2008/09 were La $Niña$ years. Here, a correlation of ^{85}Kr concentrations with the monsoon is expected, as has been reported in the northern hemisphere by (Hirota et al., 2004). Another potential effect for seasonal variations of atmospheric ^{85}Kr concentrations in Adelaide is an existing seasonalityin ^{85}Kr emissions of the two major European reprocessing plants La Hague and Sellafield.

3.3. Difference between northern and southern hemisphere

The major sources of ^{85}Kr are situated at ground level in the northern hemisphere. Hence it is often used to test atmospheric circulation models, to calculate exchange times between the hemispheres and to investigate stratosphere-troposphere exchange [29][30][31]. Using ^{85}Kr as a dating tracer, we can investigate the relation between northern and southern hemispheric activity concentration , that is, if an atmospheric ^{85}Kr input function for the southern hemisphere can be derived from data of northern hemispheric monitoring stations, in order to close data gaps and to optimize the monitoring network.

The northern hemispheric data set used for comparison includes measurements conducted at various locations in central Europe between 1959 and 1976 (in the following called Early measurements) as well as:

i)The data set of the Freiburg monitoring station, where sampling started in June 1973;

ii) All data from the Schauinsland station, which is active since February 1976; and

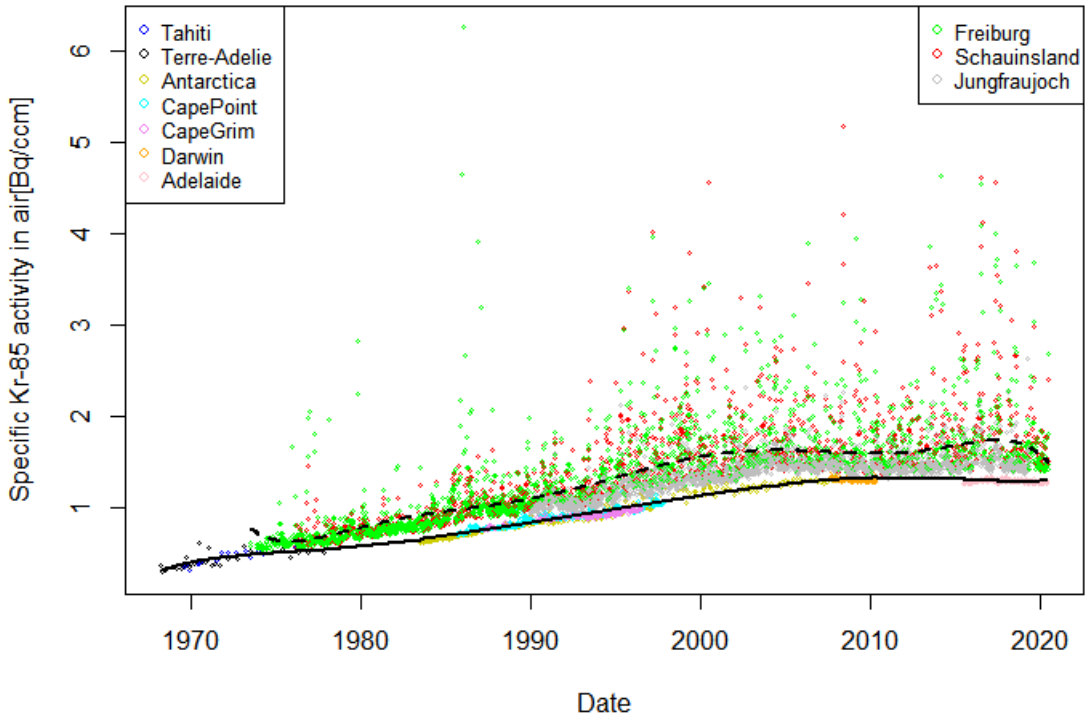

FIG. 8: Fitted 7-degree curve for both Southern and Northern hemispheric data.

iii) The monitoring station at Jungfraujoch where sampling started in January 1990 [18]. This northern hemispheric data set comprises around 6000 ^{85}Kr measurements done over 60 years and the southern hemispheric data set more than 1300 ^{85}Kr measurements conducted over the past 50 years.

It should be noted that the northern hemispheric data set shows a high variability in the weekly averaged ^{85}Kr samples (Fig. 7). The spikes mostly result from emissions from the nearby nuclear reprocessing plants La Hague (France) and Sellafield (UK). For comparison with the southern hemisphere, the undisturbed northern hemispheric ^{85}Kr concentration is of relevance which is assumed to be represented by the baseline of the northern hemispheric data set. This baseline is represented by a 7th degree polynomial fit to the minimum ^{85}Kr values measured within a quarter of a year at all three northern hemispheric monitoring stations combined. On average, the southern hemispheric ^{85}Kr activity concentration is 11.6 $\pm$ 4.6% lower than in the undisturbed northern hemisphere. However, since January 2000, the southern hemispheric ^{85}Kr activity concentration has not been less than 90% of the activity concentration on the northern hemisphere, due to decreasing global ^{85}Kr emissions.

3.4. Calculating an interhemispheric exchange time

For calculating interhemispheric exchange time τ_{ex} the simplistic approach of a 2 box model is taken just like many previous data sets [29][30][31][24]. Assuming equal air mass in each hemisphere, equal time independent air mass flux across the equator $\frac{1}{\tau_{ex}}$ and all ^{85}Kr sources (S) to reside in the northern hemisphere, the differential equations governing the ^{85}Kr concentration change in each hemisphere are:

$$\frac{dC^{NH}}{dt} = -\lambda C^{NH} - \frac{C^{NH} - C^{NH}}{\tau_{ex}} + S^{NH} \tag{8}$$

$$\frac{dC^{SH}}{dt} = -\lambda C^{SH} + \frac{C^{NH} - C^{SH}}{\tau_{ex}} \tag{9}$$

with λ as the decay constant of ^{85}Kr and τ_{ex} as the interhemispheric exchange time. Without knowing the source term, τ_{ex} can be calculated directly from Equation 9 as

$$\tau_{ex} = \frac{C^{NH} - C^{SH}}{\frac{dC^{SH}}{dt} + \lambda C^{SH}} \tag{10}$$

Upon averaging over the past 50 years, we get interhemispheric exchange time = 1.25 years.

Usually interhemispheric exchange time values vary between 0.7 years derived from atmospheric models [32] and 1.6 years from atmospheric measurements of SF_6 [30].But our values of exchange time are long calculated compared to those determined through atmospheric modelling. This is probably because presumably both ^{85}Kr emitters and sampling stations are located near earth's surface. As interhemispheric mixing takes place mostly in the upper troposphere and lower stratosphere (UNSCEAR 2000) the time for vertical mixing of ^{85}Kr is included in our estimate.

3.5 Calculating ^{85}Kr emissions

^{85}Kr emissions can be derived from the measured ^{85}Kr activity concentrations by the atmospheric two box model approach . By inserting Equation 10 in Equation 8, we have as

$$S^{NH} = \frac{d}{dt}C^{NH} + \frac{d}{dt}C^{SH} + \lambda(C^{NH} + C^{SH}) \tag{11}$$

where S^{NH} is the source term.

The latest published global ^{85}Kr emissions are from 2010 indicating an ongoing decrease in global ^{85}Kr emissions.

V. CONCLUSION:

Using the time series of ^{85}Kr concentrations, we found the a seventh degree polynomial to model the data. Describing the data as a seventh degree polynomial, reduces the need to have the most recent air measurements. By comparison with the northern hemispheric data sets of Freiburg, Schauinsland and Jungfraujoch an interhemispheric exchange time of 1.25 years can also be calculated.

Acknowledgments

We would like to thank our project guide Dr. Rituparna Sen for her fruitful guidance and helpful suggestions. We also grateful to our fellow friends and seniors of Indian Statistical Institute, Bengaluru for their supports.

---

[1] Kersting, Schlosser, Bollhöfer, Suckow, Evaluating 5 decades of atmospheric ^{85}Kr measurements in the southern hemisphere to derive an input function for dating water and ice with implications for interhemispheric circulation and the global ^{85}Kr emission inventory, Journal of Environmental Radioactivity 225 (2020).

Click Here

[2] Singh, Balraj, Chen, Jun, 2014. Nuclear Data Sheets for A = 85. Nuclear Data Sheets, pp. 1 – 162.

Click Here

[3] Delbart, C., Barbecot, F., Valdes, D., Tognelli, A., Fourre, E., Purtschert, R., Couchoux, L., Jean-Baptiste, P., 2014. Investigation of young water inflow in karst aquifers using SF6–CFC–3H/He–85Kr–39Ar and stable isotope components. Appl. Geochem. 164 – 176.

Click Here

[4] Mayer, A., Sültenfu ß , J., Travi, Y., Rebeix, R., Purtschert, R., Claude, C., La Salle, C., Miche, H., Conchetto, E., 2014. A multi-tracer study of groundwater origin and transit-time in the aquifers of the Venice region (Italy). Appl. Geochem. 177 – 198.

Click Here

[5] Loosli, H.H., Heimann, Martin, Oeschger, Hans, 1980. Low-Level Gas Proportional Counting in an Underground Laboratory. Cambridge University Press, pp. 461 – 469.

Click Here

[6] Chen, C.Y., Li, Y.M., Bailey, K., O ' Conner, T.P., Young, L., Lu, Z.-T., 1999. Ultrasensitive isotope trace analyses with a magneto-optical trap. Am. Assoc. Adv. Sci. 1139 – 1141.

Click Here

[7] Zappala, J.C., Bailey, K., Mueller, P., O ' Connor, T.P., Roland, Purtschert, 2017. Rapid Processing of 85Kr/Kr Ratios Using Atom Trap Trace Analysis. Wiley Online Library, pp. 2553 – 2558.

Click Here

[8] Lu, Z.-T., Schlosser, P., Smethie, J.W., Sturchio, N.C., Fischer, T.P., Kennedy, B.M., Purtschert, R., Severinghaus, J.P., Severinghaus, D.K., T. Tanhua and others, 2014. Tracer applications of noble gas radionuclides in the geosciences. Earth Sci. Rev. 196 – 214.

Click Here

[9] Aoki, Nobuyuki, Yoshihiro, Makide, 2005. " The concentration of krypton in the atmosphere — its revision after half a century — . Chem. Lett. 1396 – 1397.

Click Here

[10] Sartorius, H., Schlosser, C., S Schmid, W., 2002. Weiss Verfahren zur Bestimmung der Aktivit ¨ atskonzentration der atmosph ¨ arischen Edelgase Krypton-85 und Xenon-133, Blatt 3.4. 9. Loseblattsammlung FS-78-15-AKU Empfehlungen zur Überwachung der .

Click Here

[11] Purtschert, Roland, Yokochi, R., Sturchio, N.C., 2013. Krypton-81 dating of old groundwater. Chapter 5. In: Isotope Methods for Dating Old Groundwater.

Click Here

[12] Styra, B., Butkus, Donatas, 1991. Geophysical Problems of Krypton-85 in the Atmosphere.

Click Here

[13] Ahlswede, Jochen, Simon, Hebel, Kalinowski, Martin, Ross, Ole, 2009. " Update of the global krypton-85 emission inventory. " Carl-Friedrich-von-Weizs ¨ acker-Zentrum für Naturwissenschaft und Friedensforschung der Universit ¨ at Hamburg.

Click Here

[14] Hippel, Frank, Albright, David H., Levi, Barbara G., 1985. Stopping the production of fissile

materials for weapons. Sci. Am. 40 – 47.

Click Here

[15] Winger, K., Feichter, Johann, Kalinowski, M.B., Sartorius, H., Schlosser, C., 2005. A new compilation of the atmospheric 85krypton inventories from 1945 to 2000 and its evaluation in a global transport model. J. Environ. Radioact. 183 – 215.

Click Here

[16] Kalinowski, Martin B., Feichter, Johann, Nikkinen, Mika, Schlosser, Clemens, 2006. Environmental sample analysis. In: Verifying Treaty Compliance, pp. 367 – 387.

Click Here

[17] Kalinowski, Martin B., Sartorius, Hartmut, Uhl, Stefan, Weiss, Wolfgang, 2004. Conclusions on plutonium separation from atmospheric krypton-85 measured at various distances from the Karlsruhe reprocessing plant. J. Environ. Radioact. 203 – 222.

Click Here

[18] Bollhöfer, A., Schlosser, C., Schmid, S., Konrad, M., Purtschert, R., Krais, R., September 2019. Half a century of Krypton-85 activity concentration measured in air over Central Europe: trends and relevance for dating young groundwater. J. Environ. Radioact. 205 – 206, 7 – 16.

Click Here

[19] Ahlswede, Jochen, Simon, Hebel, Ross, Ole J., Schoetter, Robert, Kalinowski, Martin B., 2013. Update and improvement of the global krypton-85 emission inventory. J. Environ. Radioact. 34 – 42.

Click Here

[20] Schoeppner, Michael, Glaser, Alexander, 2016. Present and future potential of krypton- 85 for the detection of clandestine reprocessing plants for treaty verification. J. Environ. Radioact. 300 – 309.

Click Here

[21] Farges, L., Patti, F., Gros, R., Bourgeon, P., 1974. Activite du krypton-85 dans l ' air hemispheres Nord et Sud. J. Radioanal. Chem. 147 – 155.

Click Here

[22] Patti, F., Bourgeon, P., 1980. Concentrations atmospheriques de 85 Kr dans les hemispheres nord et sud. J. Radioanal. Chem. 221 – 228.

Click Here

[23] Weiss, W., Sartorius, H., Levin, I., Francey, R.J., 1996. Atmospheric 85Kr at Cape Grim. In: Francey, R.J., Dick, A.L., Derek, N. (Eds.), Baseline Atmospheric Program Australia 1994-95. Click Here

[24] Bollhöfer, A., Schlosser, C., Ross, O.J., Sartorius, H., Schmid, S., 2014. Variability of atmospheric krypton-85 activity concentrations observed close to the ITCZ in the southern hemisphere. J. Environ. Radioact. 111 – 118.
Click Here

[25] Schlosser, C., Bollhöfer, A., Schmid, S., Krais, R., Bieringer, J., Konrad, M., 2017. Analysis of radioxenon and Krypton-85 at the BfS noble gas laboratory. Appl. Radiat. Isot. 16 – 19.
Click Here

[26] Kersting, Arne, Sofia Brander, and Axel Suckow. "Modelling 85Kr Datasets with python for Applications in Tracer Hydrology and to Investigate Atmospheric Circulation. " MethodsX, (in press).

[27] Doering, Che, Saey, Paul, 2014. Hadley cell influence on 7Be activity concentrations at Australian mainland IMS radionuclide particulate stations. J. Environ. Radioact. 88 – 94.
Click Here

[28] Wu, Xiaokang, Yang, Huang, Waugh, Darryn W., Orbe, Clara, Tilmes, Simone, Lamarque, Jean Francois, 2018. Spatial and temporal variability of interhemispheric transport times. Atmos. Chem. Phys. 7439 – 7452.
Click Here

[29] Ross, Ole, 2010. Simulation of Atmospheric Krypton-85 Transport to Assess the Detectability of Clandestine Nuclear Reprocessing. Hamburg University Hamburg.
Click Here

[30] Levin, Ingeborg, Hesshaimer, Vago, 1996. Refining of atmospheric transport model entries by the globally observed passive tracer distributions of 85krypton and sulfur hexafluoride (SF6). J. Geophys. Res.: Atmosphere 16745 – 16755.
Click Here

[31] Weiss, W., Sartorius, H., Stockburger, H., 1992. Global Distribution of Atmospheric 85 Kr. A Database for the Verification of Transport and Mixing Models.
Click Here

[32] Aghedo, A., Rast, S., Schultz, M.G., 2008. Sensitivity of tracer transport to model resolution,

forcing data and tracer lifetime in the general circulation model ECHAM5. Atmos. Chem. Phys. Discuss. 137 – 160.

Click Here

[33] Li, Hu, Ditaranto, Willson, Yan, Optimization of Cryogenic CO_2 Purification for Oxy-coal Combustion, Energy Procedia, August (2013).

Click Here